CrossMark

ORIGINAL PAPER

Modelling and optimization of syngas production by methane dry reforming over samarium oxide supported cobalt catalyst: response surface methodology and artificial neural networks approach

Bamidele V. Ayodele[1,2] · Maksudur R. Khan[1,2] · Safdar Sk Nooruddin[3] · Chin Kui Cheng[1,2]

Abstract The reforming of methane by carbon dioxide for the production of syngas is a potential technological route for the mitigation of greenhouse gases. However, the process is highly endothermic and often accompanied by catalyst deactivation from sintering and carbon deposition. Besides, the applications of dissimilar catalytic systems in methane dry reforming have made it difficult to obtain generalized optimum conditions for the desired products. Hence, optimization studies of any catalytic system often resulted in a unique optimum condition. The present study aimed to investigate optimum conditions of variables such as methane (CH_4) partial pressure, carbon dioxide (CO_2) partial pressure and reaction temperature that will maximize syngas yields from methane dry reforming over samarium oxide supported cobalt (Co/Sm_2O_3) catalyst. The Co/Sm_2O_3 catalyst was synthesized using wet-impregnation method and characterized by thermogravimetric analysis), field emission scanning electron microscopy, energy-dispersive X-ray spectroscopy, X-ray powder diffraction and nitrogen (N_2) physisorption. Syngas production by methane dry reforming over the synthesized Co/Sm_2O_3 catalyst was investigated in a stainless steel fixed-bed reactor. The process variables (CH_4 partial pressure, CO_2 partial pressure and reaction temperature) for the syngas production were optimized using response surface methodology (RSM). The RSM and artificial neural networks (ANNs) were used to predict the syngas production from the experimental data. The comparative analysis between the two models showed that the ANN model has better prediction of the syngas yields compared to the RSM model as evident from the good agreement between the observed and the predicted values. At maximum desirability value of 0.97, optimum CH_4 and CO_2 partial pressures of 47.9 and 48.9 kPa were obtained at reaction temperature of 735 °C resulting in syngas yield of ∼79.4 and 79.0% for hydrogen (H_2) and carbon monoxide (CO), respectively.

✉ Chin Kui Cheng
bamidele.ayodele@uniben.edu; chinkui@ump.edu.my

1 Faculty of Chemical and Natural Resources Engineering, Universiti Malaysia Pahang, Lebuhraya Tun Razak, 26300 Gambang, Kuantan, Pahang, Malaysia

2 Center of Excellence for Advanced Research in Fluid Flow, Lebuhraya Tun Razak, 26300 Gambang, Kuantan, Pahang, Malaysia

3 Department of Chemical Engineering, King Faisal University, Al Hasa, Saudi Arabia

Introduction

Synthesis gas (syngas) is a mixture of H_2 and CO used as chemical intermediate for the production of wide range of oxygenated fuels and valuable chemicals such as dimethyl ethers and methanol (Rostrup-Nielsen 2000; Chawl et al. 2012). The production of syngas on commercial scale has been through steam reforming of natural gas and coal gasification employing supported nickel catalysts (Lu and Lee 2007; Kopyscinski et al. 2010). This process is, however, constrained by problems such as catalyst deactivation from sintering, coking and poisoning (Sehested 2006; Lakhapatri and Abraham 2009). In addition, these

processes are major contributors to greenhouse gases, a major cause of global warming (Figueroa et al. 2008; Martavaltzi et al. 2010). Besides, the syngas produced via these processes do not have the required ratios to be used as feed stock for the production of oxygenated hydrocarbons (Inderwildi et al. 2008).

Recently, there has been growing research interest in the production of syngas from methane dry reforming due to its advantages over the existing processes (Horváth et al. 2011; Ayodele and Cheng 2015). One of such advantages is the potential of the process to mitigate greenhouse effect by utilizing CH_4 and CO_2 as feed stock for syngas production (Braga et al. 2014). Moreover, syngas with low H_2: CO ratio suitable for the production of synthetic liquid fuels and oxygenated chemicals via Fischer–Tropsch synthesis (FTS) is produced (Khodakov et al. 2007; Wang et al. 2012). However, one major drawback for developing this technology into large-scale production is catalyst deactivation (Lee et al. 2014). In order to overcome this challenge, the synthesis of metal catalysts such as platinum (Pt), palladium (Pd), ruthenium (Ru), rhodium (Rh), nickel (Ni) and cobalt (Co) on magnesium oxide (MgO) (Fan et al. 2011), cerium oxide (CeO_2) (Ayodele and Cheng 2015), zirconium oxide (ZrO_2) (Özkara-Aydınoğlu and Aksoylu 2010), aluminium oxide (Al_2O_3), (Foo et al. 2011; Ferencz et al. 2014), neodymium oxide (Nd_2O_3) (Ayodele et al. 2016b), praseodymium oxide (Pr_2O_3) (Ayodele et al. 2016c), lanthanium oxide (La_2O_3) (Ayodele et al. 2016d) and silicon dioxide (SiO_2) (Bouarab et al. 2004), supports have been reported for methane dry reforming with results showing variation in activities of the catalysts in terms of conversion and yield.

One way to improve the catalytic system and the activities without increasing the cost of experimentation is through modelling and optimization. Modelling and optimization strategies such as empirical and phenomenological have been employed for methane dry reforming (Larentis et al. 2001). However, these mathematical-based optimization methods are very rigorous and time consuming and often do not represent the interactions between the catalyst systems which will invariably leads to misrepresentation. These challenges can be overcome by employing response surface methodology (RSM) which has the advantages of evaluating the interaction effects of the factors on the responses. Moreover, the RSM could help in obtaining models that aid in predicting the optimum conditions suitable for the desirable response. Furthermore, the relationship between factors in a nonlinear system such as catalytic reaction can be studied using artificial neural networks (ANNs). ANN has been applied for modelling processes such as hydrogen production from natural gas steam reforming, propane dehydration over Pt–Sn/Υ-

Al_2O_3 catalyst and adsorption of Cu(II) from industrial leachate by pumice, to name a few (Turan et al. 2011; Amini et al. 2013; Zamaniyan et al. 2013). To the best of the authors' knowledge, application of ANN and RSM for modelling and optimization of syngas production from methane dry reforming over Co/Sm_2O_3 catalyst has not been reported.

In this study, a novel Co/Sm_2O_3 catalyst was synthesized via wet-impregnation method and subsequently characterized for physicochemical properties using instrument techniques such as TGA, N_2 physisorption, XRD, FESEM and EDX analyses. The synthesized Co/Sm_2O_3 catalyst was employed in methane dry reforming reaction for the production of syngas in a stainless steel fixed-bed continuous flow reactor. The effects of parameters such as the reactants (CH_4 and CO_2) partial pressure, reaction temperature and feed ratios on the syngas (H_2 and CO) yields were investigated in the methane dry reforming. The design of experiment was performed in accordance with Box–Behnken design (BBD), a form of response surface methodology (RSM). The optimum conditions for the production of syngas from methane dry reforming over the Co/Sm_2O_3 were predicted using the BBD model and compared with ANN model. The main objective of the present study is to investigate the optimum conditions for syngas production by methane dry reforming over a novel Co/Sm_2O_3 catalyst. In addition, the predictive modelling of the syngas production by methane dry reforming over the catalyst was also investigated using ANN and BBD.

Experimental

Catalyst synthesis

Prior to the synthesis of the catalyst, the Sm_2O_3 support was prepared by thermal decomposition of samarium(III) nitrate hexahydrate (99.99% purity, Sigma-Aldrich) at 500 °C for 2 h (Hussein et al. 2003; Mohammadinasab et al. 2014; Ayodele et al. 2016a). The Sm_2O_3-supported Co catalyst was synthesized by wet-impregnation method. The Co/Sm_2O_3 mixture was obtained by the addition of aqueous solution of cobalt(II)nitrate hexahydrate (99.99% purity Sigma-Aldrich) containing equivalent of 20 wt% cobalt loading to the Sm_2O_3 powder under magnetic stirring for 3 h. Consecutively, the slurry was oven-dried for 24 h at 120 °C, crushed and finally calcined at 600 °C for 6 h to obtain $20wtCo/Sm_2O_3$.

Catalytic activity test

Figure 1 shows the schematic representation of the experimental set-up for the production of syngas from methane
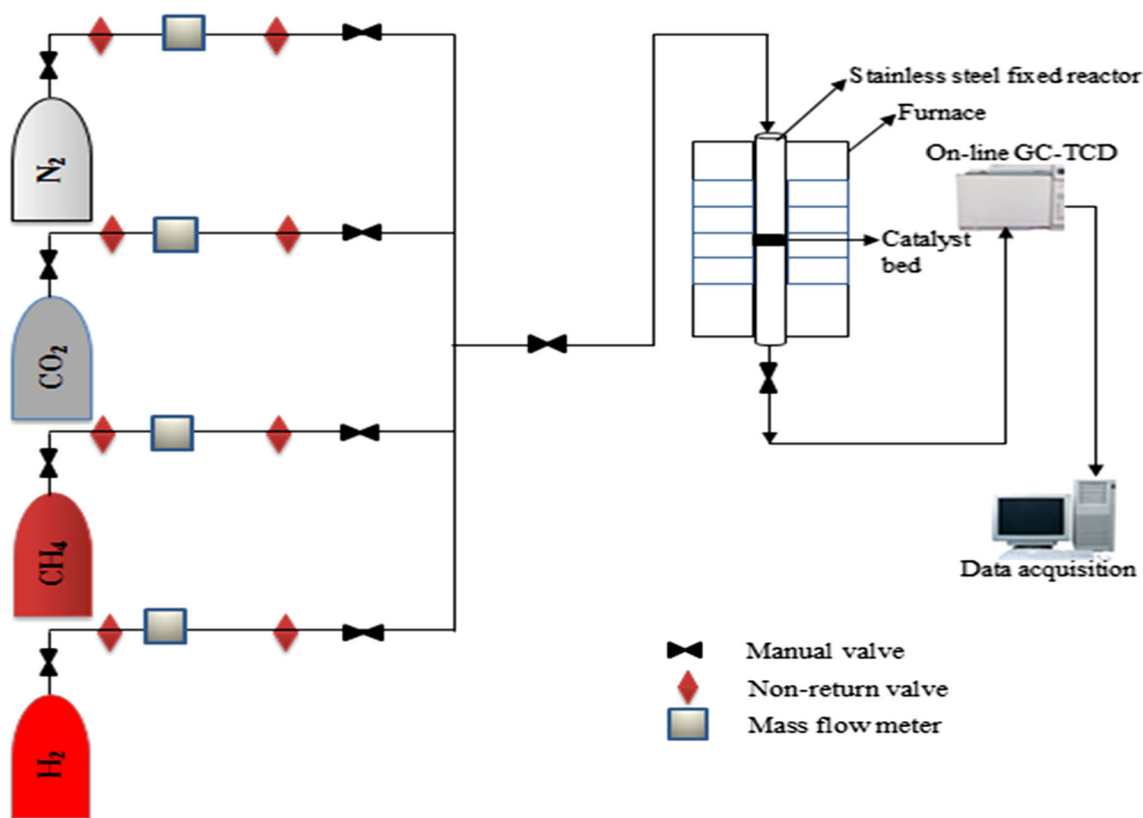
Fig. 1 Schematic diagram of experimental set-up for the syngas production from methane dry reforming

dry reforming over the 20wt%Co/Sm_2O_3 catalyst. The set-up comprised CO_2 and CH_4 which are the main reactants for the dry reforming process, as well as N_2 and H_2 which serves as the carrier gas and for reduction, respectively. The continuous fixed-bed reactor was loaded with 200 mg of catalysts supported with quartz wool placed vertically inside a split-tube furnace. The temperature of the catalytic bed was monitored using K-type thermocouple. The catalyst was reduced in 60 ml min^{-1} of 20% H_2 and 80% N_2 prior to the commencement of the catalytic activity test. The flow rate of the inlet gas was maintained at 100 ml min^{-1} and individually regulated with the aid of Alicat digital mass flow controller (MFC). The outlet gas products composition (CO_2, CH_4, CO and H_2) was measured with gas chromatography (GC) equipped with thermal conductivity detector (TCD). Two packed columns were used, viz. Supelco Molecular Sieve 13 × (3.1 m × 0.0032 m OD × 0.002 m ID, 60/80 mesh, stainless steel) and Agilent Hayesep DB (9.1 m × 0.0032 m OD × 0.002 m ID, 100/120 mesh, stainless steel). He gas was used as a carrier with flowrate of 20 ml min^{-1} with operating column temperature of 120 °C and detector temperature of 150 °C (column pressure <90 psi). Separation and quantification of gas analytes, viz. hydrogen (H_2), methane (CH_4) and carbon dioxide (CO_2) were performed using

Hayesep DB column, while CO was analysed using the Molecular Sieve 13× column. The conversion of CH_4 and CO_2 and the yields of H_2 and CO were calculated using Eqs. (1)–(4).

$$CH_4 \text{ conversion } (\%) = \frac{F_{CH_{4in}} - F_{CH_{4out}}}{F_{CH_{4in}}} \times 100 \qquad (1)$$

$$CO_2 \text{ conversion } (\%) = \frac{F_{CO_{2in}} - F_{CO_{2out}}}{F_{CO_{2in}}} \times 100 \qquad (2)$$

$$H_2 \text{ yield} = \frac{F_{H_{2out}}}{2 \times F_{CH_{4in}}} \times 100 \qquad (3)$$

$$CO \text{ yield} = \frac{F_{CO_{out}}}{F_{CH_{4in}} + F_{CO_{2in}}} \times 100 \qquad (4)$$

where $F_{CO_{2in}}, F_{CH_{4in}}, F_{CO_{2out}}, F_{CH_{4out}}$ are the inlet and outlet molar flow rates of CO_2 and CH_4, respectively; $F_{H_{2out}}$, and $F_{CO_{out}}$, are the outlet molar flow rate of H_2 and CO, respectively.

Catalyst characterization

Thermal behaviour of the freshly prepared 20 wt%Co/Sm_2O_3 catalyst was performed by thermogravimetric analyzer (Q-500 series) under N_2 atmosphere. The TG and DTG of the temperature programmed calcination of the

catalyst were collected by heating about 5 mg of the sample up to 1000 °C at a heating rate of 10 °C min^{-1}. The crystallites and phase identification of the catalyst were analysed by X-ray powder diffraction using RIGAKU Miniflex II X-ray diffractometer capable of measuring powdered diffraction pattern from 3° to 145° in 2θ scanning range. The X-ray source is Cu K-alpha with wavelength (λ) of 0.154 nm radiation. The XRD is equipped with the latest version of PDXL, RIGAKU full function powder-diffraction analysis software. The textural property analysis of the catalyst was done by N_2 adsorption–desorption measurement. The catalyst sample was degassed at 250 °C prior to analysis. The BET specific surface area and the pore volume were determined from the adsorption–desorption isotherm. The morphology and the elemental composition of the as-prepared catalyst were determined using JEOL field emission scanning electron microscopy (FESEM) equipped with energy-dispersive X-ray spectroscopy (EDX).

Response surface design of experiments

The experimental design for the optimization study was performed employing a three-factor, three-level BBD, a form of RSM design. BBD was employed for the experimental design due to its feasibility, simplicity, efficiency and its application for modelling systems without extreme conditions (Shiva et al. 2014; Ayodele and Cheng 2015). Extreme conditions refer to corner points and star points which are points selected from experimental values. In addition, BBD also offers the advantages of fewer experimental runs for three factors which can be used to explore a quadratic response surfaces and create a second-order polynomial model. In this study, the individual and interaction effects of the reactants partial pressures and the reaction temperature on syngas yields were investigated using BBD. The BBD experiment was designed using Statistica version 13 (Dell corps, USA) (refer to Table S1). The BBD design is made up of 51 runs consisting of CH_4 partial pressure (10–50 kPa), CO_2 partial pressure (10–50 kPa) and reaction temperature (650–750 °C). A RSM second-order polynomial equation shown in Eq. (5) was employed for fitting the experimental data in order to match the relationship between the input variables and the responses.

$$Y_i = \beta_o + \sum_{j=1}^{k} \beta_j x_j + \sum_{j=1}^{k} \beta_{jj} x_j^2 + \sum \sum_{i<j}^{k} \beta_{ij} x_i x_j \tag{5}$$

where Y_i, β_o, β_j, β_{jj} and β_{ij} are the predicted responses, the offset term, the linear effect, the square effect and the interaction effect, respectively.

Artificial neural networks modelling

The ANNs were employed to develop a nonlinear model using the neural networks toolbox made of input, hidden (consisting of weight and bias) and output layers located in the MATLAB software environment (Joo et al. 2015). The inputs parameters into the ANNs are the reactants (CH_4 and CO_2) partial pressures and the reaction temperature, while the output layers are the syngas yields. The hidden neurons representing the data between the input and output layers are scaled within the range of −1 and 1 using a hyperbolic tangent function (activation function) depicted in Eq. (6). The ways the neurons are link to each other significantly influence the performance of ANN. In the present study, the input parameters were modelled in such a way to cause the summing mechanism of the next neuron with a view to choosing the highest probability for the output (Agatonovic-Kustrin and Beresford 2000). Each input data set is assigned a weight which is iteratively adjusted to minimize the training error. The ANN model was configured using feed forward algorithm. The choice of feed forward configuration is due to its wide applications in industrial processes (Scott et al. 2007). In addition, the feed forward configuration is easy to implement in variety of chemical processes. The feedforward ANN was trained using Levenberg–Marquardt expression (Eq. (7)) to ensure accurate prediction of the model. The training was performed by inputting a "training dataset to the ANN network" (Scott et al. 2007; Zamaniyan et al. 2013). During the training, the ANN matches the input and output values in order to minimize the difference between the predicted and the targeted values (Agatonovic-Kustrin and Beresford 2000). Consequently, the training algorithm was employed to adjust the network's interconnection weights in order to reduce the prediction errors that might occur from the trained dataset. The errors of the difference between the input data and the output value were estimated using MSE defined in Eq. (8) (Zamaniyan et al. 2013). The ANN training and modelling was performed using the neural network toolbox in MATLAB computing environment (The Mathworks, Inc. version 2010a)

$$F(n) = \frac{2}{1 + e^{-2n}} - 1 \tag{6}$$

where n is the number of neuron.

$$(J^t J + \lambda I)\delta = J^t \in \tag{7}$$

where J is the Jacobian matrix for process, λ is the Levenberg's damping factor, δ is the weight update vector, and E is the output vector.

$$MSE = \frac{1}{N} \sum_{i=1}^{N} (X_i - Y_i)^2 \tag{8}$$

where N, X_i and Y_i are the number of data required for the network training, the input data and the output data, respectively.

Results and discussions

Catalyst characterization

The TG and DTG curves obtained from the temperature programmed calcination of the freshly prepared Co/Sm_2O_3 catalyst are depicted in Fig. 2a. Seven peaks representing weight losses of each component in the catalyst mixture with respect to temperature can be identified from the DTG curves. The first three peaks (I-III) at temperature ranged 80–200 °C can be attributed to the sequential loss of physical and hydrated water leading to the formation of anhydrous $Co(NO_3)_2$. Further increase in temperature leads to sequential thermal decomposition of the anhydrous $Co(NO_3)_2$ represented by peaks IV-VI at temperature ranged 200–400 °C to obtain Co_3O_4. This implies that the catalyst is in its pure state at temperature >400 °C which informed the choice of setting the calcination temperature at 500 °C.

The XRD pattern of the as-prepared catalyst is depicted in Fig. 2b. The spinel Co_3O_4 crystal can be identified at
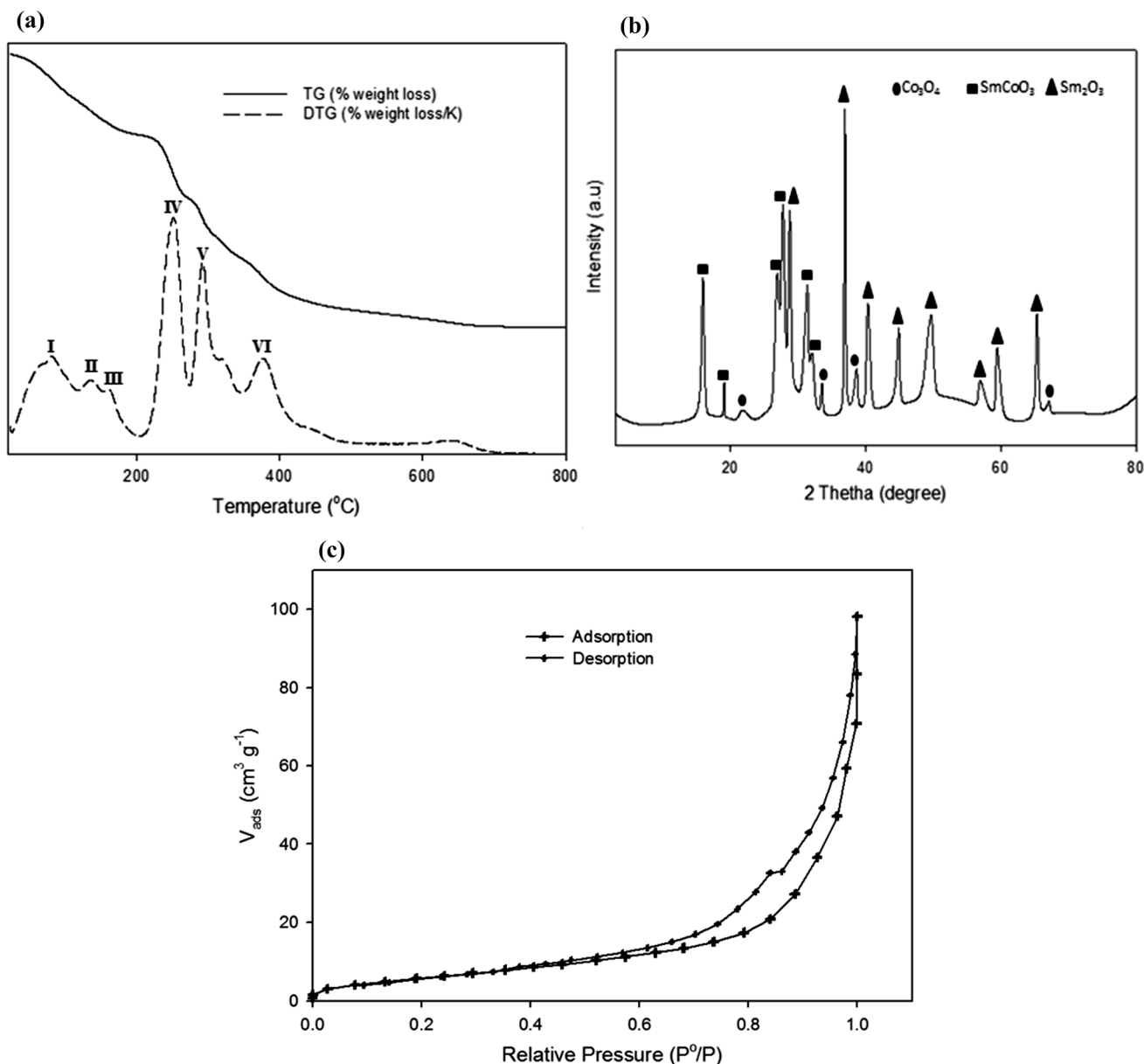

Fig. 2 **a** TG and DTG profiles for temperature programmed calcination, **b** XRD pattern and **c** N_2 adsorption–desorption isotherm of the fresh 20 wt%Co/80 wt%Sm_2O_3 catalyst

$2\theta = 21.70°$, $33.53°$, $38.67°$ and $67.14°$ representing (1 3 1), (2 1 1), (2 2 2) and (1 3 1) lattice planes of body-centred cubic and faced-centred cubic structures of Co_3O_4, respectively. The Sm_2O_3 crystal particles can be identified at $2\theta = 28.74°$, $36.87°$, $40.29°$, $44.91°$, $49.68°$, $56.79°$ $59.33°$ and $65.33°$ representing (1 0 1), (1 1 1), (2 0 1), (4 0 1), (3 3 1), (1 1 2), (5 1 1) and (4 4 0) lattice plane of body-centred cubic, hexagonal and face-centred cubic structures of Sm_2O_3, respectively. The interaction between Co_3O_4 and Sm_2O_3 leads to the formation of perovskite $SmCoO_3$ which can be identified at $2\theta = 15.87°$, $19.02°$, $26.89°$, $27.73°$, $31.36°$, $32.08°$ representing (1 0 0), (1 1 1), (1 0 1), (1 1 0), (2 2 0) and (2 0 0) lattice plane of body-centred cubic, hexagonal and faced-centred cubic structures of perovskite $SmCoO_3$. The crystallite size of the Sm_2O_3 was estimated as 46.56 nm from full width half maximum (FWHM) of the (1 1 1) peak. Figure 2c shows the N_2 adsorption–desorption isotherm of the freshly prepared catalyst. It can be seen that the isotherm displayed type-IV curve with H2 hysteresis based on IUPAC classification signifies uniform mesopores within the sample. BET specific surface area of 23.05 m^2 g^{-1} was obtained for the freshly prepared 20 wt%Co/Sm_2O_3 catalyst.

The EDX micrograph and the FESEM image of the freshly prepared 20 wt%Co/Sm_2O_3 catalyst are depicted in Fig. 3. It can be seen that part of the 20 wt%Co/Sm_2O_3

Fig. 3 a EDX micrograph and FESEM image, b EDX-dot mapping of the fresh 20 wt%Co/80 wt%Sm_2O_3 catalyst
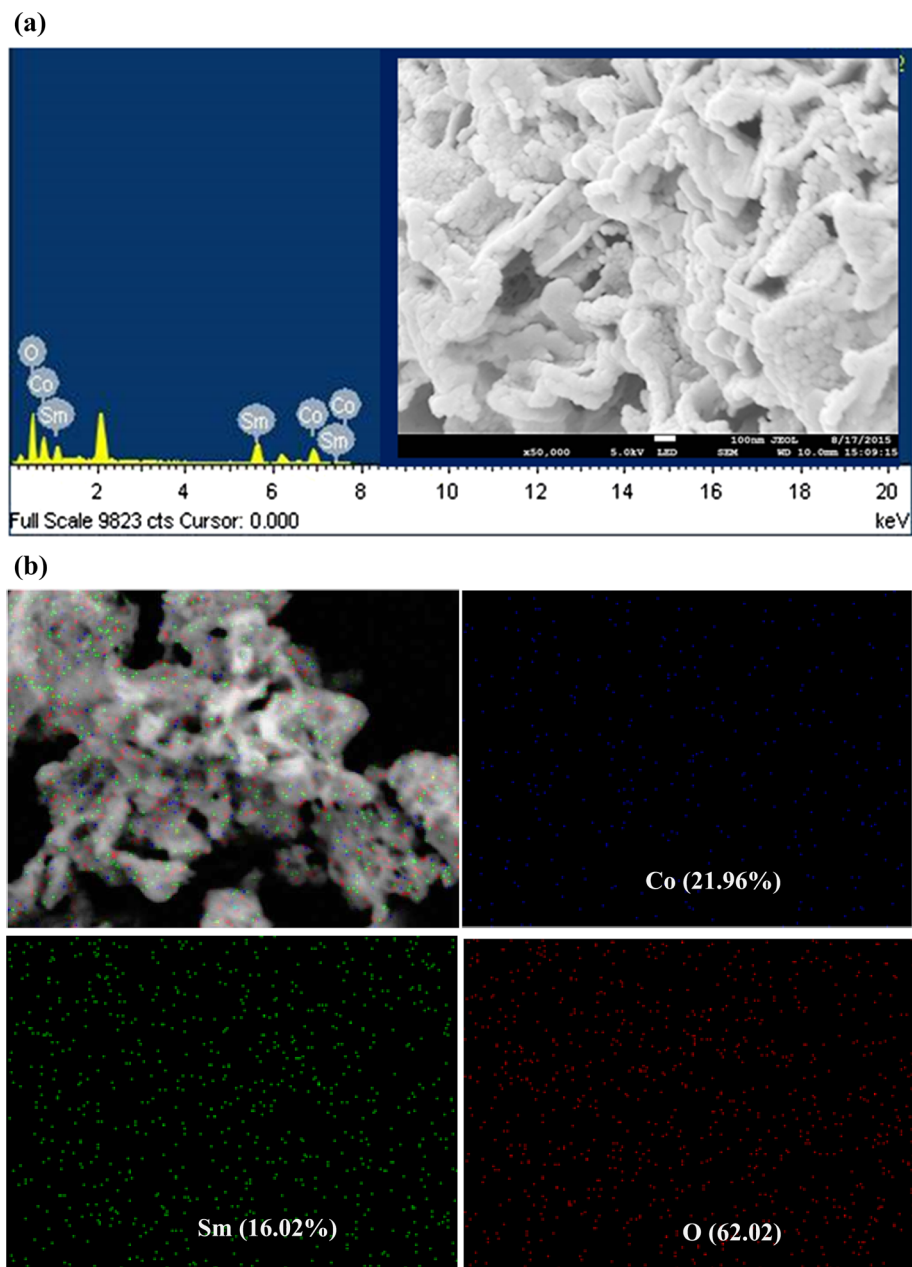
particles are spherically shaped with evidence of weak agglomeration. The elemental composition of 21.96 and 78.08% obtained for Co and Sm_2O_3 from the EDX analysis is consistent with the stipulated amount of the as-prepared 20 wt%Co/Sm_2O_3 catalyst. The EDX-dot mapping depicted in Fig. 3b shows that the Co species are uniformly distributed on the Sm_2O_3 support which is consistent with the XRD pattern of the fresh Co/Sm_2O_3 catalyst.

Response surface methodology

Effect of reactant partial pressure and reaction temperature on syngas yield

The three-dimensional response plots showing the effects of the reactants (CH_4 and CO_2) partial pressure on the syngas yields are depicted in Fig. 4. Interestingly, the H_2 yields are significantly influenced by changes in CH_4 partial pressure and the reaction temperature (cf. Fig. 4a–c). The increase in the CH_4 partial pressure leads to corresponding increase in the H_2 yields as shown in Fig. 4a. This could be attributed to dissociation of methane ($CH_4 \rightarrow C + H_2$) on the surface of the catalyst leading to increase in the H_2 yields. This observation is consistent with the literature where methane dissociations have been reported as the rate determining steps in dry reforming reactions (Nandini et al. 2006; Cui et al. 2007; Pakhare et al. 2014). Similarly, increase in temperature significantly increases the H_2 yields (Fig. 4c). This could be due to the substantial effects of temperature on the conversion of methane leadings to increase in H_2 yields which is consistent with Arrhenius behaviour for temperature-dependent chemical reaction (Senum and Yang 1977). The effect of CO_2 partial pressure on H_2 yield was insignificant between 10 and 20 kPa; however, there was a marginal significant increase in H_2 yield at CO_2 partial pressure of 30–50 kPa (cf. Fig. 4a, c). Furthermore, CO yields significantly increase with both CO_2 partial pressure and temperature (Fig. 4d–f). The increase in CO yields with CO_2 partial pressure and temperature could be as results of the CO_2 dissociation on the catalyst surface. According to Cui et al. (2007), the dissociation of CO_2 ($CO_2 \rightarrow CO + 1/2O_2$) is thermodynamically favoured at temperature ranged 550–750 °C with the release of surface O_2 to neutralized the effect of coke deposited from sides reaction such as methane cracking and reverse Boudouard. The ANOVA results shown in Table 1 revealed that the three factors are statistically significant in the production of syngas from methane dry reforming over the Co/Sm_2O_3 catalyst since their respective $p < 0.005$. Moreover, the interaction effect between CH_4 and CO_2 partial pressures

as well as, CH_4 partial pressure and reaction temperature are statistically significant on the H_2 yield ($p < 0.005$). However, the interaction effect between CO_2 partial pressure and reaction temperature is not statistically significant ($p > 0.005$). The CO yield is favoured by the interaction effect of CO_2 partial pressure and reaction temperature ($p < 0.005$), while the interaction effects between CH_4 partial pressure and CO_2 partial pressure are marginally significant. Moreover, the R^2 values of 0.94 and 97 obtained for the H_2 and CO yields, respectively, signify that over 90% of the experimental data were well fitted into the model. Similarly, adj-R^2 values of 0.96 and 0.97 were obtained from the RSM model for H_2 and CO yields. This implies that over 96 and 97% of variation actually explained by the independent variables (reactant partial pressures and the reaction temperature) have significant effects on the responses (H_2 and CO yields). The quadratic model of RSM obtained for H_2 and CO yields in terms of coded factors from multiple regression analysis of the experimental data is shown in Eq. (9) and (10).

$$H_2 \text{yield} = +39.42 + 31.01A + 6.28B + 33.14C + 9.95AB \\ + 5.52AC + 5.98A^2 + 2.73B^2 - 2.67C^2 \quad (9)$$

$$CO \text{ yield} = +40.46 + 5.86A + 31.69B + 33.65C \\ + 8.60AB + 4.90BC + 1.59A^2 + 6.37B^2 \quad (10)$$

Artificial neural networks modelling

The ANN model for the prediction of syngas production was developed using the 51 data sets comprised the inputs (reactants partial pressures and temperature) and the targets (syngas yield). Prior to the development of the ANN model, 75% of the data were employed for the network training while the remaining 25% were used for testing the ANN feed forward algorithm. The training of the data allows the input variables to be repeatedly iterated in such a way that the weights (bias) are adjusted based on the learning rule until the network structure has a very low MSE value (Zamaniyan et al. 2013). An initial screening of the hidden neuron that minimizes the MSE was performed. The hidden layer with 2 neuron (MSE = 7.3×10^{-9}) was selected for the network training.

Comparison of the ANN and RSM model

Comparison between the predictive capability of the ANN and RSM models for syngas production from methane dry reforming was statistically discriminated using statistical parameters such as mean absolute percentage error (MAPE), standard error of estimate (SEE), standard error

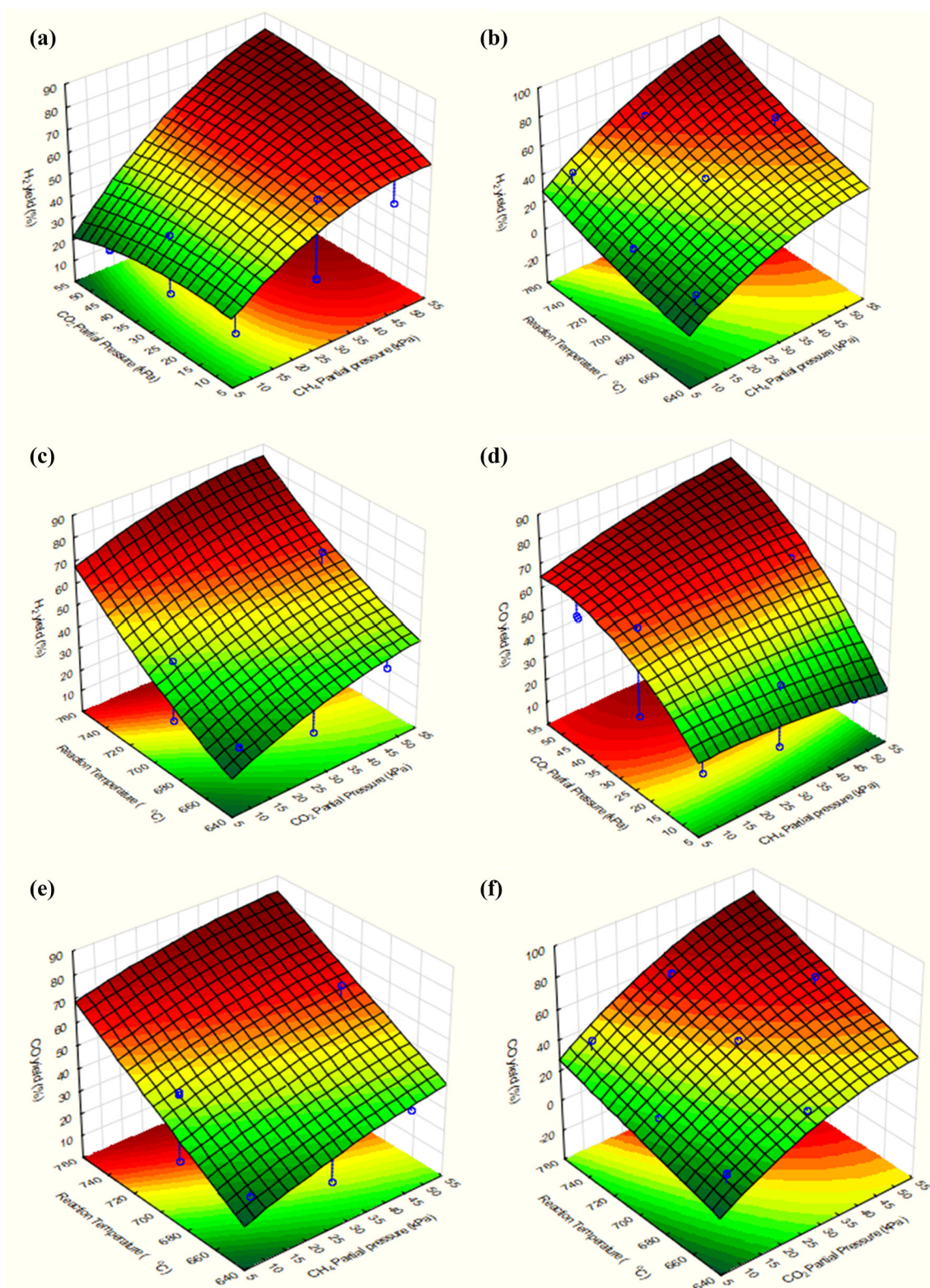**Fig. 4** Response surface plots showing the effects of **a** reactants partial pressure on H_2 yield, **b** reaction temperature and CH_4 partial pressure on H_2 yield, **c** reaction temperature and CH_4 partial pressure on H_2 yield, **d** reactants partial pressure on CO yield, **e** reaction temperature and CH_4 partial pressure on CO yield, **f** reaction temperature and CH_4 partial pressure on CO yield

Table 1 Analysis of variance of the factors used for the RSM model

FAactor	H$_2$ yield (%); R^2 = .97; Adj R^2: 0.97					CO yield (%); R^2 = 0.98; Adj R^2: 0.97				
	SS	df	MS	F	p	SS	df	MS	F	p
A	5772.20	1	5772.20	333.96	0.0000	205.69	1	205.69	14.07	0.0005
B	236.50	1	452.78	26.19	0.0000	6026.49	1	6026.49	414.19	0.0000
C	6591.55	1	6591.55	381.37	0.0000	6792.93	1	6792.93	464.62	0.0000
AB	297.51	1	297.51	33.92	0.0000	221.71	1	221.71	27.40	0.0000
AC	91.25	1	91.25	10.40	0.0025	17.62	1	17.62	2.18	0.1477
BC	12.18	1	12.18	1.39	0.2454	72.28	1	72.28	8.93	0.0047
A^2	452.78	1	452.78	26.19	0.0000	32.22	1	32.22	2.20	0.1448
B^2	94.29	1	94.29	5.46	0.0000	511.95	1	511.95	35.02	0.0000
C^2	90.36	1	90.34	5.23	0.0271	0.31	1	0.31	0.03	0.8858
Lack of fit	778.57	10	77.86	0.94	0.5109	502.99	10	50.30	0.72	0.7027
Error	359.56	41	8.77			331.70	41	8.09		
Total SS	13,992.09	50				14,228.67	50			

of prediction (SEP), mean percentage error (MPE), mean absolute error (MAE) and coefficient of determination (R^2) (Prakash Maran et al. 2013; Ayodele and Cheng 2015). The estimation of the prediction errors using the aforementioned statistical parameters helps in the quantification and better understanding of the performance of the models and their reliability. The results of the comparative statistical analysis of the models using Eqs. (11)–(16) are summarized in Table 2. It can be seen that the statistical errors of predictions of the syngas yields obtained from the ANN model were lower compared to that of RSM model in all cases. This implies that ANN model has a better capacity to predict syngas production from methane dry reforming compare to the RSM model. The better prediction capability of ANN model obtained in this study is consistent with the findings of Prakash Maran et al. (2013) and Singh et al. (2013) who employed ANN and RSM for modelling the production of l-glutamise by Bacillus cereus MTCC 1305 and for prediction of mass transfer parameters during osmotic dehydration of *Carica Papaya* L. The parity plots showing the comparison between the observed syngas

yields from the experimental runs and the predicted yields using the ANN and the RSM models are depicted in Fig. 5. It can be seen that the ANN model closely predict the syngas yields compared to the RSM model. This could be attributed to the high tendency of the ANN model to approximate the nonlinearity of the system irrespective of the order, while the RSM model is constrained to second-order polynomial (Singh et al. 2013).

$$\text{MAPE} = \frac{1}{n}\sum_{t=1}^{n}|E_t - P_t|. \tag{11}$$

$$\text{SEE} = \sqrt{\frac{\sum_{i=1}^{n}(E_t - P_t)^2}{n}} \tag{12}$$

$$\text{SEP} = \frac{\sqrt{\frac{\sum_{i=1}^{n}(E_t - P_t)^2}{n}}}{E_t} \tag{13}$$

$$\text{MPE} = \frac{100\%}{n}\sum_{t=1}^{n}\frac{E_t - P_t}{E_t} \tag{14}$$

$$\text{MAE} = \frac{1}{n}\sum_{i=1}^{n}|P_i - E_i| \tag{15}$$

$$R^2 = \frac{n\sum P_i E_{i-}(\sum P_i)(\sum E_i)}{\left(n\left(\sum P_i^2\right) - \left(\sum P_i\right)^2\right)\left((n\left(\sum E_i^2\right) - \left(\sum E_i\right)^2\right)} \tag{16}$$

where n, E_t and P_t are the total number of predictions, experimental and predicted values, respectively.

Optimization of the syngas production

The method of desirability was employed to obtain the optimum process conditions that will maximize the production of syngas from methane dry reforming over the 20

Table 2 Comparison between ANN and RSM for prediction of syngas production

Statistical parameters	H$_2$ yield (%)		CO yield (%)	
	RSM	ANNs	RSM	ANNs
SEE	3.86	1.25	3.28	1.55
SEP	21.62	1.11	15.37	2.74
MAPE	10.26	3.46	3.43	3.43
MPE	4.51	0.24	0.37	3.15
MAE	3.42	1.25	1.33	2.91
R^2	0.97	0.98	0.98	0.99
adj. R^2	0.97	0.97	0.97	0.98

(a)

(b)

(c)

Observed vs. Predicted Values
3 3-level factors, 1 Blocks, 51 Runs; MS Residual=8.090196
DV: CO yield (%)

(d)

Observed vs. Predicted Values
3 3-level factors, 1 Blocks, 51 Runs; MS Residual=8.769823
DV: H₂ yield (%)

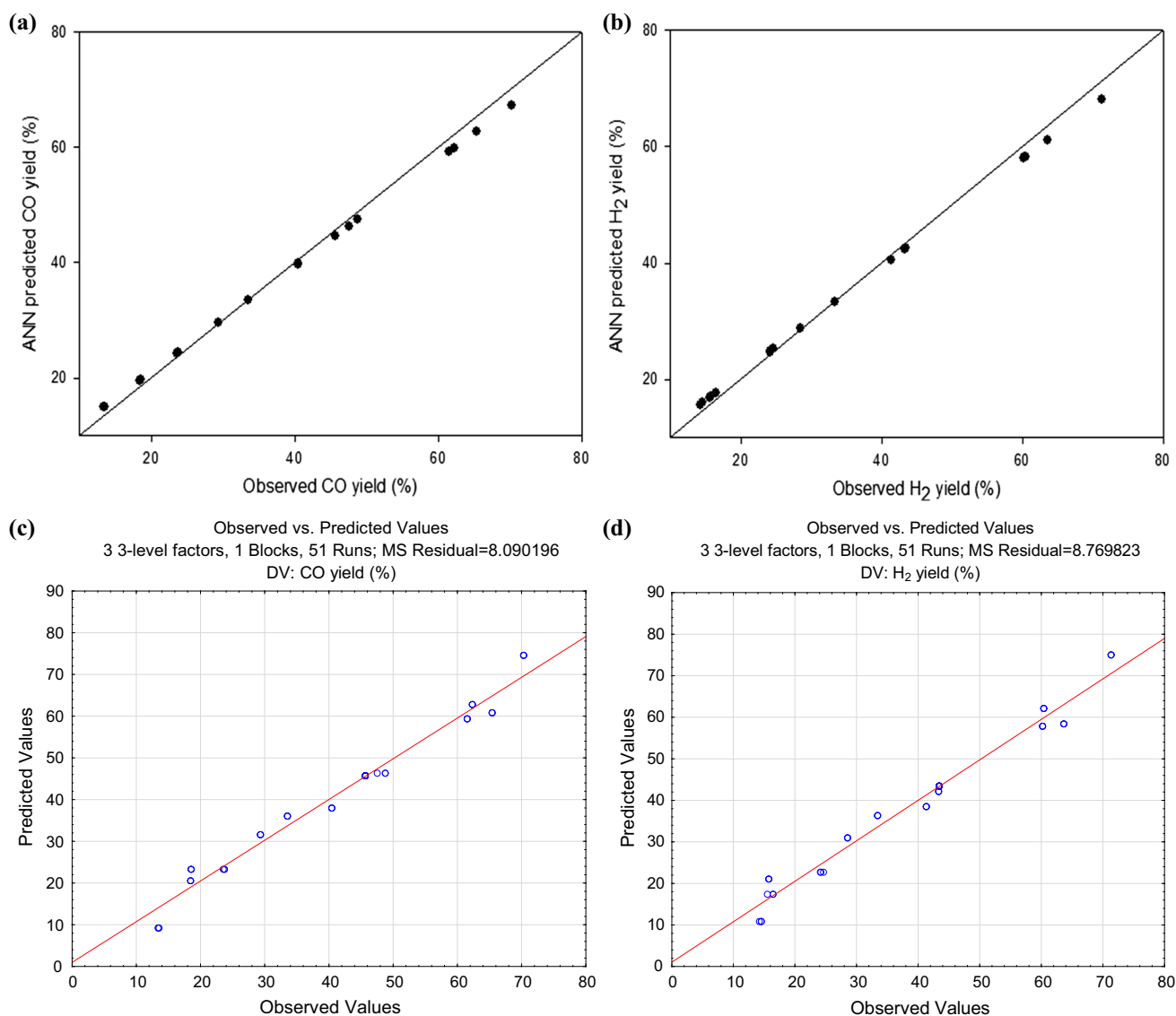**Fig. 5** Parity plots showing the comparison between the observed values and the predicted values **a** ANN model for CO yield, **b** ANN model for H$_2$ yield, **c** RSM model for CO yield, **d** RSM model for H$_2$ yield

wt%Co/Sm$_2$O$_3$ catalyst. Desirability function was employed as a tool for the optimization of the syngas production in this study due to its wide applications in industrial processes to determine the optimum conditions of multiple responses (Wang and Wan 2009). The application of desirability function often leads to the best operation conditions that provides the most desirable responses (Wu 2014). In order to maximize a response, the individual desirability is expressed in Eq. (17)

$$f_i(x_i) = \begin{cases} 0 & \text{if} \quad \chi_{i(x)} < l_i \\ \left(\dfrac{\chi_{i(x)} - l_i}{T_i - l_i}\right)^s & \text{if} \quad l_i < \chi_{i(x)} < T_i \\ 1.00 & \text{if} \quad \chi_{i(x)} > T_i \end{cases} \quad (17)$$

where χ_i, T_i, l_i are the desirability values, target values, and lower values of each of the responses, while s is a determinant reflecting how important to hit the target.

The desirability approach for optimization entails the conversion of each response to an individual desirability function within the range of 0.1–1.0. In order to obtain the optimum conditions for the syngas production, the overall desirability (the geometric sum of the individual desirability) was maximized. Table 3 shows the optimum conditions obtained for the syngas production over 20 wt%Co/Sm$_2$O$_3$ based on desirability approach. Solution one (CH$_4$ partial pressure = 47.9 kPa, CO$_2$ partial pressure = 48.9 kPa, reaction temperature = 735 °C) with

Table 3 Optimum conditions obtained based on desirability approach for syngas production over 20 wt%Co/80 wt%Sm_2O_3

Solution	CH_4 partial pressure (kPa)	CO_2 partial pressure (kPa)	Reaction temperature (°C)	H_2 yield (%)	CO yield (%)	Desirability (χ)
1	47.9	48.9	735.0	79.4	79.0	0.97
2	40.6	42.4	725.0	71.6	70.6	0.96
3	38.9	43.5	738.0	68.4	71.2	0.95
4	42.3	39.7	722.0	75.7	69.6	0.93
5	35.7	41.3	740.0	64.6	70.5	0.92
6	42.3	37.7	748.0	72.3	67.8	0.91
7	34.6	38.6	723.0	67.8	65.5	0.90
8	40.5	32.7	698.0	64.5	68.7	0.89
9	38.9	40.1	712.0	70.1	72.3	0.88
10	32.6	35.7	655.0	62.1	63.4	0.87

Table 4 Validated values of syngas yields obtained from using the optimum conditions predicted from desirability approach

Experiment run	Validation values		Absolute percentage error	
	H_2 yield (%)	CO yield (%)	H_2 yield (%)	CO yield (%)
1	78.59	78.70	1.01	0.38
2	79.16	79.12	0.29	0.15
3	78.79	78.80	0.76	0.25

desirability of 0.97 was selected as the best. The maximum overall desirability of 0.97 was obtained for the optimization of the syngas production based on the profiles for predicted values and desirability (Fig. S1). Corresponding optimum values of 47.9 kPa, 48.9 kPa and 735 °C were obtained for CH_4 partial pressure, CO_2 partial pressure and reaction temperature, respectively, at the maximum desirability. At these optimum conditions, maximum values of 79.4 and 79.0% were predicted for the H_2 and CO yields, respectively.

Validation of optimum conditions from the desirability approach

The best set of solutions obtained from the desirability functions were validated by setting those conditions in methane dry reforming triplicate experiment runs over the 20 wt%Co/Sm_2O_3 catalyst as shown in Table 4. The mean values of the absolute percentage error of deviation obtained for the H_2 and CO yields were ~ 0.68 and $\sim 0.26\%$, respectively. This implies that the best optimum conditions obtained from the models using the desirability approach is statistically reliable with over 99% confidence level for both H_2 and CO yield.

Conclusions

For the first time, a comparative approach was employed to investigate the application of ANN and RSM for modelling and optimization of syngas production by methane dry reforming over 20 wt%Co/Sm_2O_3 catalyst based on experimental data obtained from the BBD. The comparative analysis using statistical parameters shows that ANN model possesses better capability for prediction of syngas production from methane dry reforming than the RSM model. The method of the desirability function was employed to simultaneously optimize the H_2 and CO yields. Maximum desirability values of 0.97 were obtained from the profiles for predicted and desirability using RSM. The maximum H_2 and CO yields of ~ 79.4 and $\sim 79.0\%$ as well as CH_4 and CO_2 conversions of ~ 71.0 and $\sim 74.0\%$ were obtained at the following optimum conditions: CH_4 partial pressure of 47.9 kPa; CO_2 partial pressure of 48.9 kPa and reaction temperature of 735 °C. A further validation of the models showed that the predicted optimum conditions are statistically reliable with high level of confidence interval. This study has significantly contributed to finding optimum conditions of process variables (CH_4 partial pressure, CO_2 partial pressure and reaction temperature) that maximized the syngas yields obtained from methane dry reforming over Co/Sm_2O_3 catalyst.

Moreover, the application of ANN and RSM models as useful tools for modelling, prediction and optimization of syngas production from methane dry reforming over 20 wt%Co/Sm_2O_3 has been demonstrated. However, due to uniqueness of any catalytic system, the optimum conditions obtained in this study cannot be generalized.

References

Agatonovic-Kustrin S, Beresford R (2000) Basic concepts of artificial neural network (ANN) modeling and its application in pharmaceutical research. J Pharm Biomed Anal 22(5):717–727

Amini Y, Fattahi M, Khorasheh F, Sahebdelfar S (2013) Neural network modeling the effect of oxygenate additives on the performance of Pt–Sn/γ-Al$_2$O$_3$ catalyst in propane dehydrogenation. Appl Petrochemical Res. 3(1–2):47–54

Ayodele BV, Cheng CK (2015) Modelling and optimization of syngas production from methane dry reforming over ceria-supported cobalt catalyst using artificial neural networks and Box-Behnken design. J Ind Eng Chem 32:246–258

Ayodele BV, Hossain MA, Chong SL, Soh JC, Abdullah S, Khan MR, Cheng CK (2016a) Non-isothermal kinetics and mechanistic study of thermal decomposition of light rare earth metal nitrate hydrates using thermogravimetric analysis. J Therm Anal Calorim 125(1):423–435

Ayodele BV, Hossain SS, Lam SS, Osazuwa OU, Khan MR, Cheng CK (2016b) Syngas production from CO$_2$ reforming of methane over neodymium sesquioxide supported cobalt catalyst. J Nat Gas Sci Eng. 34:873–885

Ayodele BV., Khan MR, Cheng CK. Syngas production from CO$_2$ reforming of methane over ceria supported cobalt catalyst: Effects of reactants partial pressure. J Nat Gas Sci Eng. 34:873-885

Ayodele BV, Khan MR, Cheng CK (2016c) Greenhouse gases mitigation by CO$_2$ reforming of methane to hydrogen-rich syngas using praseodymium oxide supported cobalt catalyst. Clean Technol Environ Policy. Springer, Berlin Heidelberg, pp 1–13

Ayodele BV, Khan MR, Lam SS, Cheng CK (2016d) Production of CO-rich hydrogen from methane dry reforming over lanthania-supported cobalt catalyst: kinetic and mechanistic studies. Int J Hydrogen Energy 41(8):4603–4615

Bouarab R, Akdim O, Auroux A, Cherifi O, Mirodatos C (2004) Effect of MgO additive on catalytic properties of Co/SiO$_2$ in the dry reforming of methane. Appl Catal A Gen. 264(2):161–168

Braga TP, Santos RC, Sales BM, da Silva BR, Pinheiro AN, Leite ER, Valentini A (2014) CO$_2$ mitigation by carbon nanotube formation during dry reforming of methane analyzed by factorial design combined with response surface methodology. Chinese J Catal 35(4):514–523

Chawl SK, George M, Patel F, Patel S (2012) Production of Synthesis Gas by Carbon Dioxide Reforming of Methane over Nickel based and Perovskite Catalysts. Procedia Eng. 46:1–6

Cui Y, Zhang H, Xu H, Li W (2007) Kinetic study of the catalytic reforming of CH$_4$ with CO$_2$ to syngas over Ni/α-Al$_2$O$_3$ catalyst: the effect of temperature on the reforming mechanism. Appl Catal A Gen. 318:79–88

Fan MS, Abdullah AZ, Bhatia S (2011) Hydrogen production from carbon dioxide reforming of methane over Ni–Co/MgO–ZrO$_2$ catalyst: process optimization. Int J Hydrogen Energy 36(8):4875–4886

Ferencz Z, Baán K, Oszkó A, Kónya Z, Kecskés T, Erdőhelyi A (2014) Dry reforming of CH$_4$ on Rh doped Co/Al$_2$O$_3$ catalysts. Catal Today 228:123–130

Figueroa JD, Fout T, Plasynski S, McIlvried H, Srivastava RD (2008) Advances in CO$_2$ capture technology—The U.S. Department of Energy's Carbon Sequestration Program. Int J Greenh Gas. Control. 2(1):9–20

Foo SY, Cheng CK, Nguyen T-H, Adesina AA (2011) Kinetic study of methane CO$_2$ reforming on Co–Ni/Al$_2$O$_3$ and Ce–Co–Ni/Al$_2$O$_3$ catalysts. Catal Today 164(1):221–226

Horváth A, Stefler G, Geszti O, Kienneman A, Pietraszek A, Guczi L (2011) Methane dry reforming with CO$_2$ on CeZr-oxide supported Ni, NiRh and NiCo catalysts prepared by sol–gel technique: relationship between activity and coke formation. Catal Today 169(1):102–111

Hussein GAM, Buttrey DJ, DeSanto P, Abd-Elgaber AA, Roshdy H, Myhoub AYZ (2003) Formation and characterization of samarium oxide generated from different precursors. Thermochim Acta 402(1–2):27–36

Inderwildi OR, Jenkins SJ, King DA (2008) Fischer-Tropsch mechanism revisited: alternative pathways for the production of higher hydrocarbons from synthesis gas. J Phys Chem C 2008(112):1305–1307

Joo S, Yoon J, Kim J, Lee M, Yoon Y (2015) NO$_x$ emissions characteristics of the partially premixed combustion of H$_2$/CO/CH$_4$ syngas using artificial neural networks. Appl Therm Eng 80:436–444

Khodakov AY, Chu W, Fongarland P (2007) Advances in the development of novel cobalt Fischer-Tropsch catalysts for synthesis of long-chain hydrocarbons and clean fuels. Chem Rev 107(5):1692–1744

Kopyscinski J, Schildhauer TJ, Biollaz SMA (2010) Production of synthetic natural gas (SNG) from coal and dry biomass – A technology review from 1950 to 2009. Fuel 89(8):1763–1783

Lakhapatri SL, Abraham MA (2009) Deactivation due to sulfur poisoning and carbon deposition on Rh-Ni/Al$_2$O$_3$ catalyst during steam reforming of sulfur-doped n-hexadecane. Appl Catal A Gen. 364(1–2):113–121

Larentis AL, de Resende NS, Salim VMM, Pinto JC (2001) Modeling and optimization of the combined carbon dioxide reforming and partial oxidation of natural gas. Appl Catal A Gen 215(1–2):211–224

Lee JH, You YW, Ahn HC, Hong JS, Kim SB, Chang TS, Suh JK (2014) The deactivation study of Co–Ru–Zr catalyst depending on supports in the dry reforming of carbon dioxide. J Ind Eng Chem 20(1):284–289

Lu Y, Lee T (2007) Influence of the Feed Gas Composition on the Fischer-Tropsch Synthesis in Commercial Operations. J Nat Gas Chem 16(4):329–341

Martavaltzi CS, Pampaka EP, Korkakaki ES, Lemonidou AA (2010) Hydrogen Production via Steam Reforming of Methane with Simultaneous CO$_2$ Capture over CaO − Ca$_{12}$Al$_{14}$O$_{33}$. Energy Fuels 24(4):2589–2595

Mohammadinasab R, Tabatabaee M, Aghaie H, Seyed Sadjadi MA (2014) A Simple Method for Synthesis of Nanocrystalline Sm$_2$O$_3$Powder by Thermal Decomposition of Samarium Nitrate. Synth React Inorganic, Met Nano-Metal Chem. 45(3):451–454

Nandini A, Pant KK, Dhingra SC (2006) Kinetic study of the catalytic carbon dioxide reforming of methane to synthesis gas over Ni-K/CeO$_2$-Al$_2$O$_3$ catalyst. Appl Catal A Gen. 308:119–127

Özkara-Aydınoğlu Ş & Aksoylu AE (2010). Carbon dioxide reforming of methane over Co-X/ZrO$_2$ catalysts (X = La, Ce, Mn, Mg, K). Catal Commun 11(15):1165–1170

Pakhare D, Schwartz V, Abdelsayed V, Haynes D, Shekhawat D, Poston J, Spivey J (2014) Kinetic and mechanistic study of dry (CO$_2$) reforming of methane over Rh-substituted La$_2$Zr$_2$O$_7$ pyrochlores. J Catal 316:78–92

Prakash Maran J, Sivakumar V, Thirugnanasambandham K, Sridhar R (2013) Artificial neural network and response surface methodology modeling in mass transfer parameters predictions during osmotic dehydration of Carica papaya L. Alexandria, Eng J, pp 507–516

Rostrup-Nielsen JR (2000) New aspects of syngas production and use. Catal Today 63(2–4):159–164

Scott DJ, Coveney PV, Kilner JA, Rossiny JCH, Alford NMN (2007) Prediction of the functional properties of ceramic materials from composition using artificial neural networks. J Eur Ceram Soc 27(16):4425–4435

Sehested J (2006) Four challenges for nickel steam-reforming catalysts. Catal Today 111(1–2):103–110

Senum GI, Yang RT (1977) Rational approximations of the integral of the Arrhenius function. J Therm Anal 11(3):445–447

Shiva M, Atashi H, Mirzaei AA, Arsalanfar M, Zare A (2014) Study of syngas conversion to light olefins by statistical models. Fuel 123:205–210

Singh P, Shera SS, Banik J, Banik RM (2013) Optimization of cultural conditions using response surface methodology versus artificial neural network and modeling of l-glutaminase production by Bacillus cereus MTCC 1305. Bioresour Technol 137:261–269

Turan NG, Mesci B, Ozgonenel O (2011) The use of artificial neural networks (ANN) for modeling of adsorption of Cu(II) from industrial leachate by pumice. Chem Eng J 171(3):1091–1097

Wang J, Wan W (2009) Application of desirability function based on neural network for optimizing biohydrogen production process. Int J Hydrogen Energy 34(3):1253–1259

Wang N, Chu W, Zhang T, Zhao XS (2012) Synthesis, characterization and catalytic performances of Ce-SBA-15 supported nickel catalysts for methane dry reforming to hydrogen and syngas. Int J Hydrogen Energy 37(1):19–30

Wu FC (2014). Optimization of Correlated Multiple Quality Characteristics Using Desirability Function. Qual Eng.119–126

Zamaniyan A, Joda F, Behroozsarand A, Ebrahimi H (2013) Application of artificial neural networks (ANN) for modeling of industrial hydrogen plant. Int J Hydrogen Energy 38(15):6289–6297